Theor Chem Acc (2011) 130:1009–1022
DOI 10.1007/s00214-011-0947-3

REGULAR ARTICLE

The geometric, energetic, and electronic properties of charged phosphorus-doped silicon clusters, PSi_n^+/PSi_n^- (n = 1–8)

Yu Chang · Guoliang Li · Aimei Gao · Hongyu Chen · Qian-shu Li

Received: 11 November 2010 / Accepted: 18 April 2011 / Published online: 29 June 2011

Abstract Charged phosphorus-doped small silicon clusters, PSi_n^+/PSi_n^- ($n = 1-8$), have been investigated using the B3LYP/6-311+G* level Kohn–Sham density functional theory (KS-DFT) method. For comparison, the geometries of neutral PSi_n clusters were also optimized at the same level, though most of them have been previously reported. According to our results, cationic PSi_n^+ clusters have ground state structures similar to those of pure silicon clusters Si_{n+1}, with the exception of $n = 5$. For anionic PSi_n^-, most of the lowest-energy structures are in accord with Wade's $2N+2$ rule for closed polyhedra: PSi_4^-, PSi_5^-, PSi_6^-, and PSi_8^-, respectively, favor the trigonal bipyramid, tetragonal bipyramid, pentagonal bipyramid, and tricapped trigonal prism (TTP) structures, corresponding to Wade's $2N+2$ rule with $N = 5$, 6, 7, and 9. The structures tend to contract when the cationic species is reduced initially to the neutral species and subsequently to the anionic species, implying a strengthening interaction between atoms within the clusters on one and two electron reductions of the cationic species to the neutral and anionic species, respectively. The relative order of stability of the PSi_n^+/PSi_n^- isomers differs from that of the PSi_n isomers. Cluster stability was also analyzed by adiabatic ionization potentials (AIP), adiabatic electron affinities (AEA), binding energies (BE), second-order energy differences (Δ_2E), and HOMO-LUMO gap values. The results indicate that PSi_4^- and PSi_7^- clusters are more stable than their neighboring anionic clusters and would be potential species for further mass spectrometric measurements.

Keywords Charged phosphorus-doped silicon clusters · Structures · Stability · Density functional theory

1 Introduction

Since the discovery of fullerenes, people are attracted to clusters. Enormous effort has been applied, both theoretically and experimentally, to the study of silicon clusters [1–36] due to silicon belonging to the same group in the periodic table as carbon as well as the technological relevance toward the development of semiconductor materials. Many studies indicate that silicon favors sp^3-like bonding in silicon clusters, which leads to increased chemical reactivity as a result of many "dangling bonds" [4–6]. Introducing a heteroatom into silicon clusters helps to saturate these "dangling bonds" and thus stabilizes the silicon clusters, which has been confirmed by numerous investigations of doping transition metal (TM) atoms into silicon clusters to form cage-like structures [7–18]. Some main group elements, such as alkali metals [19–24], Al [25–27], Be [28], C [29], and N [30–32], are also considered as candidates for dopant atoms to improve the silicon cluster's stability. Different from TM-doped Si_n clusters, most of the main-group-element-doped Si_n clusters present similar patterns to those of Si_{n+1} clusters by substituting a main group atom for a Si atom.

Dedicated to Professor Akira Imamura on the occasion of his 77th birthday and published as part of the Imamura Festschrift Issue.

Electronic supplementary material The online version of this article (doi:10.1007/s00214-011-0947-3) contains supplementary material, which is available to authorized users.

Y. Chang · G. Li · A. Gao · H. Chen (✉) · Q. Li
Center for Computational Quantum Chemistry and School of Chemistry and Environment, South China Normal University, Guangdong, Guangzhou 510006, People's Republic of China
e-mail: hychen@scnu.edu.cn

Phosphorus is vicinal to silicon in the periodic table. As the energy crisis has deepened, silicon-based semiconductor materials have been increasingly utilized in solar cells. It is found that P impurities in silicon materials greatly impact the photoelectric conversion efficiency (PCE) of solar cells. A small amount of P in silicon-based materials improves conductivity by generating charge carriers, while too much P decreases the PCE, perhaps as a result of the formation of some deep energy levels. Phosphorus-doped silicon clusters could behave as a link between small P–Si species and bulk P–Si materials. In this paper, we focus on small size P-doped silicon clusters. To investigate the substitutional effect of P atom on the Si_n host cluster, Nigam et al. [33] performed a comparative study on isoelectronic Si_n^- and PSi_{n-1} ($2 \leq n \leq 13$) clusters and suggested that the geometries of P-substituted silicon clusters were similar to those of Si_n^- clusters. Charged PSi_n^+/PSi_n^- clusters have never been investigated to date to our knowledge. Considering that the experimental observations of the impurity-doped silicon clusters are usually based on the mass spectrometric measurements in which charged clusters can be produced and isolated, theoretical work on charged PSi_n^+/PSi_n^- clusters may be of some utility in the field of mass spectroscopy. Here, we report a computational study on the geometric and electronic properties of ionic PSi_n^+/PSi_n^- ($n = 1$–8) clusters, which focuses on how a P atom affects the geometry and stability of the Si_n clusters, and how reduction and oxidation impacts the structure and properties of the PSi_n clusters.

2 Computational details

Density functional theory with the 6-311+G* basis set, as implemented in the GAUSSIAN 03 program package [37], was used for all calculations. The B3LYP exchange–correlation functional [38], which includes a mixture of the Hartree–Fock exchange, the Becke three-parameter nonlocal exchange functional (B3) [39], and the Lee–Yang–Parr nonlocal correlation functional (LYP) [40], was selected. Considering computational efficiency and accuracy, the DFT-B3LYP method has been well documented as a result of its successful application to some small-sized heteroatom-doped Si clusters [14, 27, 33, 41–44]. The 6-311G specifies the McLean-Chandler (*12s9p*)/[*6s5p*] basis sets for both Si and P atoms [45]. Because of the inclusion of both cations and anions in this study, the 6-311G basis sets were augmented with *d*-polarization functions and diffuse *sp*-functions [46].

To assess the nature of the stationary points, harmonic vibrational frequencies were computed using analytic gradient techniques [47, 48]. Spin-restricted wave functions were used for all closed-shell systems, and spin-unrestricted references were employed for the open-shell species.

In order to check the reliability of our computational method, the ionization potentials (IPs) and electron affinities (EAs) of Si and P atoms were calculated. Our calculated values are IP(Si) = 8.11 eV, EA(Si) = 1.33 eV, IP(P) = 10.39 eV, and EA(P) = 0.91 eV, which are in excellent agreement with the available experimental values of 8.15 and 1.39 eV for a silicon atom plus 10.49 and 0.77 eV for a phosphorous atom [49–51], respectively. The geometries and energies of the Si_2 and Si_2^- dimers are also considered. The ground state of Si_2 favors the triplet state over the singlet by 0.70 eV. The Si–Si distance and dissociation energy for the triplet state are predicted to be 2.28 Å and 3.06 eV, respectively. These values agree well with the available experimental values: 2.25 Å bond length; 3.33 eV bond energy [52]. The Si_2^- anion favors doublet spin multiplicity for the ground state configuration, with a Si–Si distance of 2.20 Å, in close agreement with the 2.19 Å experimental bond length of a Si_2^- anion [53, 54]; thus, the method should be suitable for investigating the geometric and electronic structures of semiconductor clusters [43, 55]. It should be noted that the B3LYP functional has many drawbacks. For example, B3LYP functional is weak in treating van der Waals interactions, which could be better treated by the M05 and M06 meta hybrid functionals developed by Truhlar's group [56–60]. The LYP correlation functional is not able to treat the disperson forces responsible for the binding in noble gas dimers, the stacked benzene dimer, and base stacked nucleic acid dimers, trimers and tetramers. The B3PW91 functional [61–63] would give better description for such systems [64], and some of our results for B3PW91 are also presented (*vide post*). The optimized effective potential (OEP) method, developed by Bartlett's group [65, 66], has been called the gold standard for DFT, the so-called ab initio DFT method. On the other hand, the B3LYP functional has been shown to underestimate the energy of charge transfer electronic excitations. To fix the problems with the underestimation of charge transfer electronic excitations, some improved functionals such as CAM-B3LYP [67, 68] by Handy's group and CAM-BLYP [69] by Tozer's group have been developed.

3 Results and discussion

3.1 Structures

The geometries of PSi_n, PSi_n^-, PSi_n^+ ($n = 1$–8) clusters were optimized using the method described above. For comparison, neutral PSi_n clusters were also considered at the same level. The initial configurations were obtained in three ways: (i) replacing a Si atom with a P atom at each position of the low-energy Si_{n+1} structures (as shown in

Fig. S1 in supporting information), (ii) capping or trapping a Si atom to the low-energy PSi_{n-1} structures, and (iii) adding a P atom to the ground state structure of Si_n clusters at each possible position. This approach was also applied for the anions and the cations, after adding/removing an electron to/from the neutral clusters. For each structure, two electronic states with different multiplicities, *i.e.* the doublet and quartet states for neutral PSi_n, the singlet and triplet states for ionic PSi_n^-/PSi_n^+, were considered.

Figures 1 and 2 illustrate some low-energy structures of the PSi_n, PSi_n^-, and PSi_n^+ clusters (n = 1–5, and 6–8, respectively). All structures were confirmed to be local minima by the absence of imaginary vibrational frequencies and are designated as **xy-z**, where **x** is the total number of Si atoms, **y** becomes **n** for neutral, **a** for anionic, and **c** for cationic, and **z** represents the relative stability of the structure; as **z** decreases, stability increases. Table 1 shows the relative energies for the low-energy isomers, both with and without zero-point vibrational energy (ZPVE) corrections. It is seen that the ZPVEs have less pronounced effect on the relative energies, so we will mainly use the values without ZPVE corrections in the following discussion, unless otherwise indicated. The optimized parameters for the ground state structures are given in Table 2.

3.1.1 n = 1

After optimization, the PSi dimer was found to prefer the doublet $^2\Pi$ state as the ground state (**1n-1** in Fig. 1). As shown in Table 2, a PSi bond length of 2.089 Å was determined, which is slightly larger than 2.00 Å value obtained by Nigam et al. [33] at the B3LYP/6-31+G* level of theory; their predicted P–Si dissociation energy was 3.42 eV, whereas our calculated value of 3.55 eV is more consistent with the experimental value [70] of 3.63 eV. For PSi^- and PSi^+ ions, the optimized bond lengths are 2.019 and 2.247 Å, respectively; shorter than the neutral for the anion, longer for the cation. This can be explained by their electronic configurations: the ground $^2\Pi$ state of PSi has a $1\sigma^2 2\sigma^2 3\sigma^2 4\sigma^2 1\pi^4 5\sigma^2 2\pi^4 6\sigma^2 7\sigma^2 8\sigma^2 9\sigma^2 3\pi^3$ electronic configuration, where the highest-occupied molecular orbital (HOMO) $3\pi^3$ is a singly occupied bonding molecular orbital (MO). Therefore, taking away an electron weakens the P-Si bond; adding an electron strengthens it.

3.1.2 n = 2

Neutral PSi_2 favors the closed isosceles triangle **2n-1**, analogous with that of the Si_3^- cluster [26, 33], as the most

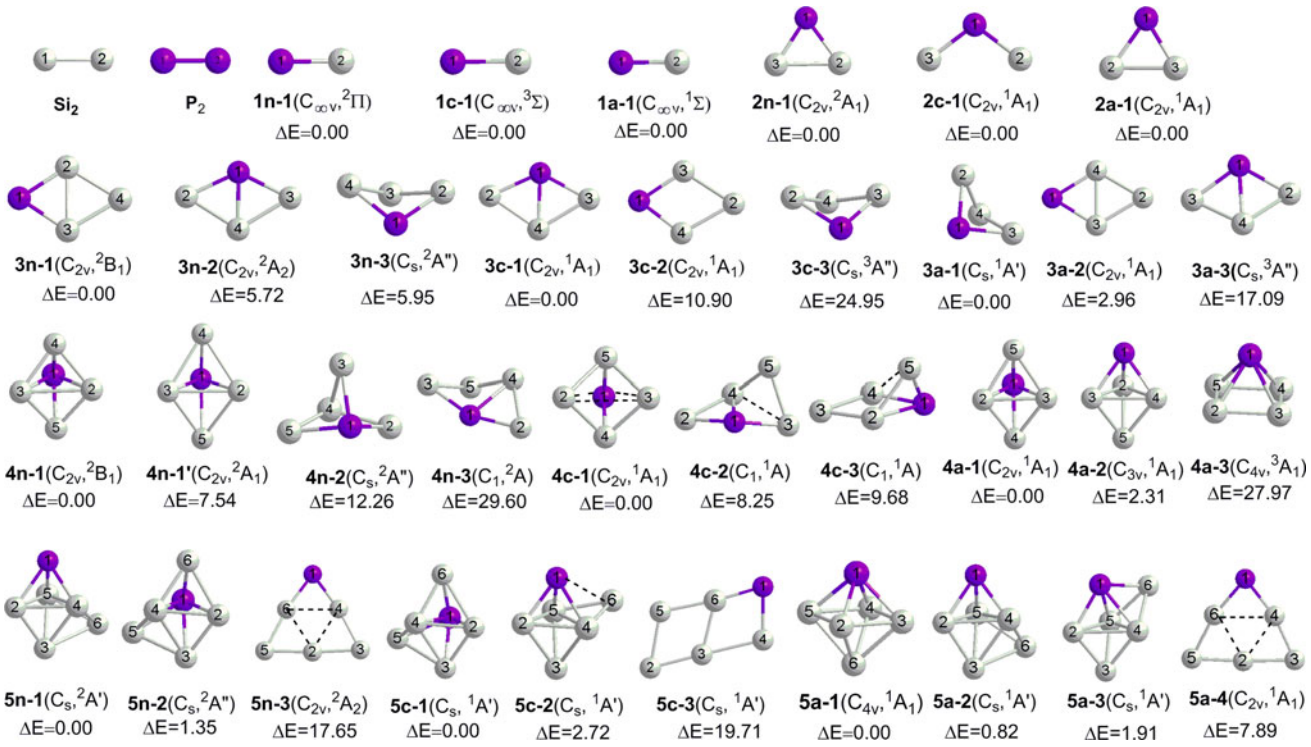

Fig. 1 Optimized geometries of the $PSi_n/PSi_n^+/PSi_n^-$ (n = 1–5) clusters at the B3LYP/6-311+G* level. The purple and light gray balls represent the P atom (marked "1") and Si atoms, respectively. All structures are designated as **xy-z**, where **x** is the total number of Si atoms, **y** becomes **n** for neutral, **a** for anionic, and **c** for cationic, and **z** represents the relative stability of the structure; as **z** decreases, stability increases

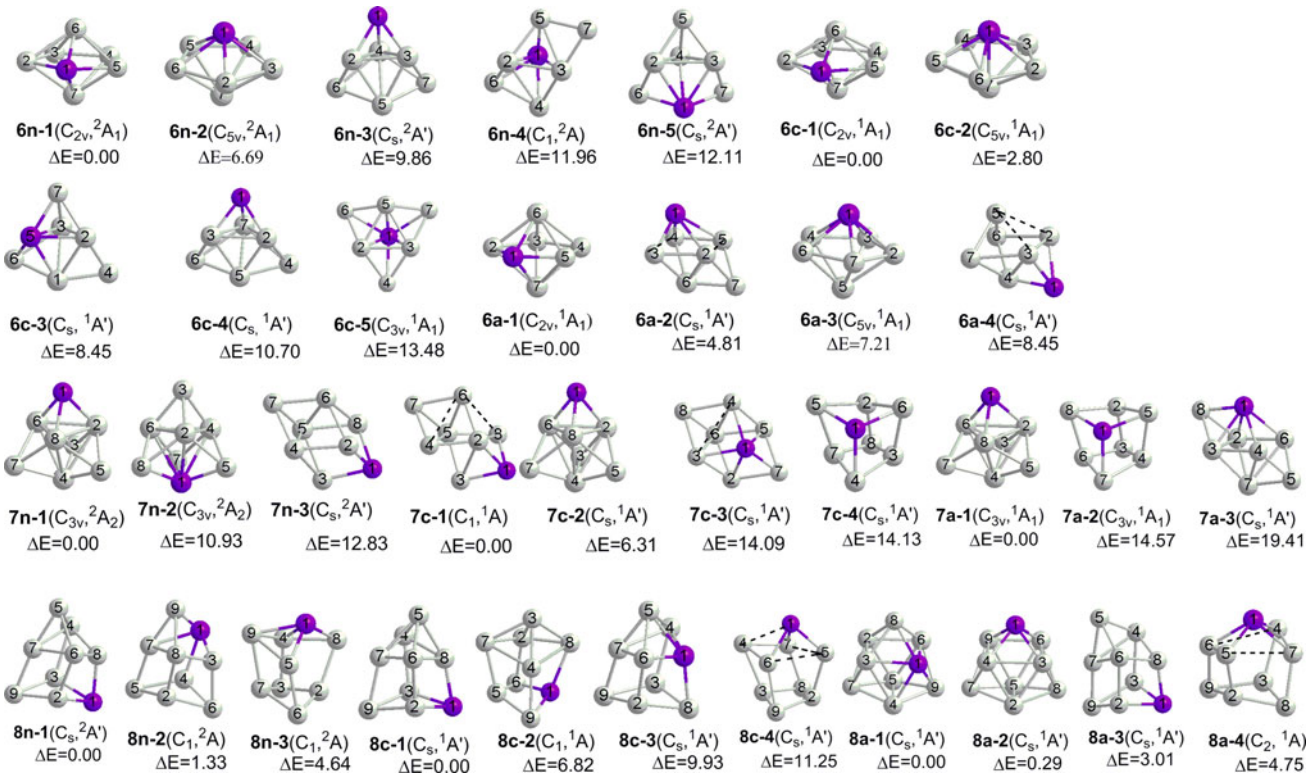

Fig. 2 Optimized geometries of the $PSi_n/PSi_n^+/PSi_n^-$ ($n = 6$–8) clusters at the B3LYP/6-311+G* level

stable structure, close to the corresponding results obtained by Nigam et al. [33]. The PSi_2 cluster is quite different from the NSi_2 cluster despite both N and P being group V elements; the NSi_2 cluster has a linear ground state structure with the *N* atom between the two Si atoms, perhaps as a result of their atomic configurations. The PSi_2^- cluster also adopts a closed isosceles triangle structure. However, the PSi_2^+ cluster forms an open isosceles triangle structure, similar to that of the isoelectronic Si_3 cluster [26, 33]. Our results indicate that adding an electron to the PSi_2 cluster compresses the triangle, whereas removing an electron expands the triangle, indicating that the interaction between the two Si atoms is strengthened as the number of electrons increases.

3.1.3 n = 3

The ground state of the neutral PSi_3 cluster displays a planar rhombus configuration (**3n-1** in Fig. 1), the P atom occupying the long diagonal vertex. It has a $^2A'$ electronic state with C_{2v} symmetry. Other low-energy isomers include the C_{2v} rhombus configuration, **3n-2**, and the C_s bent rhombus, **3n-3**, in both of which the P atom is located at the short diagonal vertex. Isomers **3n-2** and **3n-3** are almost isoenergetic, with energies 5.72 and 5.95 kcal/mol higher than **3n-1**, respectively. The results reveal that the P atom seems to prefer the lower coordination position: 2-coordinated in **3n-1** over 3-coordinated in **3n-2**.

Cationic PSi_3^+ favors the planar rhombus configuration **3c-1**, as the most stable structure, with the P atom preferring the short diagonal vertex, as in **3n-2**. Both the Si2-Si4 and P-Si2 bond lengths in **3c-1** are elongated, compared with those in neutral **3n-1.** Structure **3c-1** is analogous with the ground state structure of Si_4 [26, 33]. The second stable structure, **3c-2**, is a distorted rhombus, similar to **3n-1,** with the P atom at the long diagonal vertex, implying that the removal of an electron from the neutral cluster reverses the relative order of isomer stability. **3c-3,** the third stable isomer, is a tridimensional bent rhombus, analogous with **3n-3,** with 24.95 kcal/mol more energy than **3c-1**.

For PSi_3^-, a tridimensional bent rhombus **3a-1** with C_s symmetry, similar to **3n-3**, is preferred over the planar structure of the neutral PSi_3 and cationic PSi_3^+ clusters. It also differs from the neutral and ionic $NaSi_3$, KSi_3, $AlSi_3$, CSi_3 [22, 23, 27, and 29] clusters, which all adopt the planar rhombus structure as their ground state structure. The P-Si2 and Si2-Si4 bond lengths in **3a-1** are shortened, compared with those in the neutral and cationic equivalents. The C_{2v} planar rhombus structure, **3a-2**, similar to structure **3n-1**, has 2.96 kcal/mol more energy than **3a-1**. The other planar rhombus structure, **3a-3**, similar to **3n-2**, has 17.09 kcal/mol higher energy than **3a-1**. The addition of an electron to the

Table 1 Relative energies (in kcal/mol) for the low-energy isomers of the $PSi_n/PSi_n^+/PSi_n^-$ (n = 1–8) clusters at the B3LYP/6-311+G* level

Cluster	Neutral				Cation				Anion			
	Isomer	State	ΔE_1	ΔE_2	Isomer	State	ΔE_1	ΔE_2	Isomer	State	ΔE_1	ΔE_2
$PSi^{(\pm)}$	**1n-1**	$^2\prod$	0.00	0.00	**1c-1**	$^3\sum$	0.00	0.00	**1a-1**	$^1\sum$	0.00	0.00
$PSi_2^{(\pm)}$	**2n-1**	$^2A_1$	0.00	0.00	**2c-1**	$^1A_1$	0.00	0.00	**2a-1**	$^1A_1$	0.00	0.00
$PSi_3^{(\pm)}$	**3n-1**	$^2B_1$	0.00	0.00	**3c-1**	$^1A_1$	0.00	0.00	**3a-1**	$^1A'$	0.00	0.00
	3n-2	$^2A_2$	5.72	5.38	**3c-2**	$^1A_1$	10.90	10.92	**3a-2**	$^1A_1$	2.96	2.87
	3n-3	$^2A'$	5.95	5.90	**3c-3**	$^3A''$	24.95	24.79	**3a-3**	$^3A''$	17.09	16.89
$PSi_4^{(\pm)}$	**4n-1**	$^2B_1$	0.00	0.00	**4c-1**	$^1A_1$	0.00	0.00	**4a-1**	$^1A_1$	0.00	0.00
	4n-1′	$^2A_1$	7.54	6.85	**4c-2**	^1A	8.25	7.69	**4a-2**	$^1A_1$	2.31	2.33
	4n-2	$^2A''$	12.26	11.94	**4c-3**	^1A	9.68	9.23	**4a-3**	$^3A_1$	27.97	27.75
	4n-3	^2A	29.60	28.84								
$PSi_5^{(\pm)}$	**5n-1**	$^2A'$	0.00	0.00	**5c-1**	$^1A'$	0.00	0.00	**5a-1**	$^1A_1$	0.00	0.00
	5n-2	$^2A''$	1.35	1.40	**5c-2**	$^1A'$	2.72	2.83	**5a-2**	$^1A'$	0.82	0.88
	5n-3	$^2A_2$	17.65	17.40	**5c-3**	$^1A'$	19.71	19.67	**5a-3**	$^1A'$	1.91	1.78
									5a-4	$^1A_1$	7.89	7.90
$PSi_6^{(\pm)}$	**6n-1**	$^2B_1$	0.00	0.00	**6c-1**	$^1A_1$	0.00	0.00	**6a-1**	$^1A_1$	0.00	0.00
	6n-2	$^2A_1$	6.69	6.71	**6c-2**	$^1A_1$	2.80	2.69	**6a-2**	$^1A'$	4.81	4.77
	6n-3	$^2A'$	9.86	9.86	**6c-3**	$^1A'$	8.45	8.39	**6a-3**	$^1A_1$	7.21	7.22
	6n-4	^2A	11.96	11.92	**6c-4**	$^1A'$	10.70	10.90	**6a-4**	$^1A'$	8.45	8.37
	6n-5	$^2A'$	12.11	12.06	**6c-5**	$^1A_1$	13.48	13.46				
$PSi_7^{(\pm)}$	**7n-1**	$^2A_2$	0.00	0.00	**7c-1**	^1A	0.00	0.00	**7a-1**	$^1A_1$	0.00	0.00
	7n-2	$^2A_2$	10.93	10.78	**7c-2**	$^1A'$	6.30	6.35	**7a-2**	$^1A_1$	14.57	14.35
	7n-3	$^2A'$	12.83	12.40	**7c-3**	$^1A'$	14.09	13.75	**7a-3**	$^1A'$	19.41	18.55
					7c-4	$^1A'$	14.13	13.64				
$PSi_8^{(\pm)}$	**8n-1**	$^2A'$	0.00	0.00	**8c-1**	$^1A'$	0.00	0.00	**8a-1**	$^1A'$	0.00	0.00
	8n-2	^2A	1.33	1.22	**8c-2**	^1A	6.82	6.66	**8a-2**	$^1A'$	0.29	0.40
	8n-3	^2A	4.64	4.31	**8c-3**	$^1A'$	9.93	9.78	**8a-3**	$^1A'$	3.01	3.73
					8c-4	$^1A'$	11.25	10.97	**8a-4**	^1A	4.75	5.40

ΔE_2 are corrected for zero-point vibrational energy (ZPVE) while ΔE_1 not

neutral cluster again appears to change the relative order of isomer stability and results in the transformation of the lowest energy structure from a planar rhombus structure to the more compact three-dimensional bent rhombus structure.

We also investigated the $PSi_3/PSi_3^+/PSi_3^-$ isomers using the B3PW91 functional and presented the results in Table 3. It looks like the B3PW91 results are much similar to the B3LYP ones considering the relative energies of different isomers.

3.1.4 n = 4

4n-1 (Figs. 1, 3), the global minimum of the PSi_4 cluster has a distorted trigonal bipyramid structure with C_{2v} symmetry, similar to the $NaSi_4$, KSi_4, $AlSi_4$, and Si_5^- clusters [22, 23, 27, 33]. The electronic state of this structure is $^2B_1$. The P atom occupies one vertex of the base isosceles triangle. Structure **4n-1** can also be regarded as a P-face-capped bent rhombus formed by four Si atoms. We also found another C_{2v} symmetry trigonal bipyramid structure, named as **4n-1′**, which is structurally much similar to **4n-1** but energetically lies above **4n-1** by 7.54 kcal/mol. Structure **4n-2** can be obtained from **3n-2** by capping a Si atom onto its bent rhombus and has 12.26 kcal/mol higher energy than the ground state, **4n-1**. A Si-edge-capped bent rhombus structure, **4n-3**, comes next in energy, but is 29.60 kcal/mol above **4n-1,** thus will not be discussed further.

When an electron is removed from the neutral PSi_4 cluster (that is, it is oxidized to the cationic species), the most stable configuration of the cationic PSi_4^+, **4c-1,** has a similar framework to the Si_5 cluster, maintaining the P-face-capped bent rhombus geometry, with the C_{2v} symmetry of **4n-1**, but with the $A_{Si2\text{-}P\text{-}Si3}$ angle and the $R_{Si3–P}$ and $R_{Si2–Si3}$ distances increased. The P atom resides at the same location as is in the neutral cluster. The other two meta-stable isomers, **4c-2** and **4c-3,** both demonstrate Si-edge-capped rhombic geometries with energies 8.25 and 9.68 kcal/mol, respectively, higher than that of **4c-1**; due to their similar energies, they are viewed as nearly degenerate

Table 2 Optimized parameters for the ground state structures of the $PSi/PSi_n^+/PSi_n^-$ ($n = 1$–8) clusters at the B3LYP/6-311+G* level

Isomer	Coord[a]	Geom.	Isomer	Coord[a]	Geom.	Isomer	Coord[a]	Geom.	Isomer	Coord[a]	Geom.
1n-1	P1–Si2	2.089		Si2–Si4	2.488	**7n-1**	P1–Si2	2.287		Si4–Si8	2.367
1c-1	P1–Si2	2.247		Si2–Si5	2.566		Si2–Si4	2.767		Si5–Si7	2.309
1a-1	P1–Si2	2.019		Si3–Si6	2.616		Si2–Si5	2.475		Si7–Si9	2.380
2n-1	P1–Si2	2.164		Si4–Si5	2.575		Si2–Si8	2.684		A213	73.8
	Si2–Si3	2.492		Si4–Si6	2.413		Si4–Si5	2.397		A293	70.2
2c-1	P1–Si2	2.123	**5c-1**	P1–Si2	2.413	**7c-1**	P1–Si2	2.184		A456	96.7
	Si2–Si3	3.394		P1–Si6	2.370		P1–Si3	2.377		A476	91.9
2a-1	P1–Si2	2.209		P1–Si4	2.491		P1–Si8	2.375	8c-1	P1–Si2	2.287
	Si2–Si3	2.364		Si2–Si3	2.344		Si2–Si3	2.646		P1–Si8	2.260
3n-1	P1–Si2	2.196		Si2–Si4	2.457		Si2–Si4	2.371		Si2–Si6	2.521
	Si2–Si3	2.420		Si2–Si6	2.688		Si2–Si6	2.372		Si2–Si9	2.404
	Si2–Si4	2.347		Si4–Si6	2.388		Si2–Si8	2.663		Si4–Si5	2.546
3c-1	P1–Si2	2.254	**5a-1**	P1–Si2	2.409		Si3–Si5	2.445		Si4–Si7	2.445
	P1–Si4	2.300		Si2–Si3	2.518		Si4–Si5	2.529		Si4–Si8	2.657
	Si2–Si4	2.402		Si2–Si6	2.501		Si4–Si7	2.496		Si5–Si7	2.555
3a-1	P1–Si2	2.240	**6n-1**	P1–Si2	2.376		Si5–Si6	2.537		Si5–Si8	2.321
	P1–Si4	2.710		P1–Si6	2.418		Si5–Si7	2.312		A213	71.5
	Si2–Si4	2.334		Si2–Si3	2.473		Si5–Si8	2.441		A293	67.5
	D1234	107.9		Si2–Si6	2.573		Si6–Si7	2.510		A456	106.4
4n-1	P1–Si2	2.542		Si3–Si4	2.450		D1257	174.1		A476	112.9
	P1–Si4	2.309		Si4–Si6	2.552		D3256	176.7	**8a-1**	P1–Si3	2.571
	Si2–Si3	2.847	6c-1	P1–Si2	2.429		D4528	171.2		P1–Si6	2.498
	Si2–Si4	2.337		P1–Si6	2.347		D6425	61.9		P1–Si8	2.452
4c-1	P1–Si2	2.827		Si2–Si3	2.505	**7a-1**	P1–Si2	2.321		Si2–Si3	2.620
	P1–Si4	2.239		Si2–Si6	2.548		Si2–Si4	2.751		Si2–Si6	2.666
	Si2–Si3	3.264		Si3–Si4	2.597		Si2–Si5	2.406		Si2–Si8	2.516
	Si2–Si4	2.334		Si4–Si6	2.503		Si2–Si8	2.808		Si3–Si4	2.758
4a-1	P1–Si2	2.436	**6a-1**	P1–Si2	2.328		Si4–Si5	2.440		Si3–Si7	2.448
	P1–Si4	2.358		P1–Si6	2.507	**8n-1**	P1–Si2	2.307		Si3–Si8	2.443
	Si2–Si3	2.608		Si2–Si3	2.421		P1–Si8	2.301		Si4–Si5	2.620
	Si2–Si4	2.374		Si3–Si4	2.374		Si2–Si6	2.507		Si5–Si7	2.499
5n-1	P1–Si2	2.380		Si2–Si6	2.647		Si2–Si9	2.408		A475	63.9
	P1–Si5	2.270		Si4–Si6	2.641		Si4–Si5	2.565			
	Si2–Si3	2.343					Si4–Si7	2.666			

Bond distances and bond angles are in Å and degrees, respectively

[a] See Figs. 1 and 2 for the atom numbering

structures. Other isomers of PSi_4^+ were also found, but all were more than 20 kcal/mol energetically less stable than **4c-1**.

The addition of an electron to the neutral **4n-1** cluster does not change the trigonal bipyramid motif, but shrinks the base triangle. The P atom in both **4n-1** and **4a-1** occupies the same position; when the P atom occupies the apex of the trigonal bipyramid (C_{4v}), it yields the metastable configuration, **4a-2**, with energy 2.31 kcal/mol greater than **4a-1**. The C_{4v} quadrangular pyramid **4a-3** follows **4a-2** as the third stable structure but lies 27.97 kcal/mol above **4a-1** in energy. The trigonal bipyramid is therefore the preferred structure for the anionic PSi_4^- cluster regardless of the position occupied by the P atom, which can perhaps be explained by Wade's rules [71, 72]. According to the rule, if a cluster has $2N+2$ skeletal electrons, where N is the number of vertices, the cluster adopts a closed polyhedron. In the PSi_4^- anion, the phosphorus atom offers three *3p* electrons, and each silicon atom gives two *3p* electrons, thus the valence electrons

Table 3 Relative energies (in kcal/mol) for the low-energy isomers of the $PSi_n/PSi_n^+/PSi_n^-$ ($n = 3,4$) clusters with the 6-311+G* basis set

Neutral					Cation				Anion			
Cluster	Isomer	State	ΔE_1	ΔE_2	Isomer	State	ΔE_1	ΔE_2	Isomer	State	ΔE_1	ΔE_2
$PSi_3^{(\pm)}$	**3n-1**	$^2B_1$	0.00	0.00	**3c-1**	$^1A_1$	0.00	0.00	**3a-1**	$^1A'$	0.00	0.00
	3n-2	$^2A_2$	5.73	5.82	**3c-2**	$^1A_1$	10.90	11.03	**3a-2**	$^1A_1$	2.96	2.97
	3n-3	$^2A''$	5.95	6.29	**3c-3**	$^3A'$	24.97	23.69	**3a-3**	$^3A''$	17.10	16.81
$PSi_4^{(\pm)}$	**4n-1**	$^2B_1$	0.00	0.00	**4c-1**	$^1A_1$	0.00	0.00	**4a-1**	$^1A_1$	0.00	0.00
	4n-1'	$^2A_1$	7.54	7.62	**4c-2**	^1A	8.26	11.49	**4a-2**	$^1A_1$	2.31	3.18
	4n-2	$^2A''$	12.26	14.92	**4c-3**	^1A	9.69	12.38	**4a-3**	$^3A_1$	27.97	29.35
	4n-3	^2A	29.60	35.48[a]								

The ΔE_1 values are given by the B3LYP method while the ΔE_2 values by B3PW91

[a] Based on the B3PW91 single-point energy at the B3LYP optimized **4n-3** structure

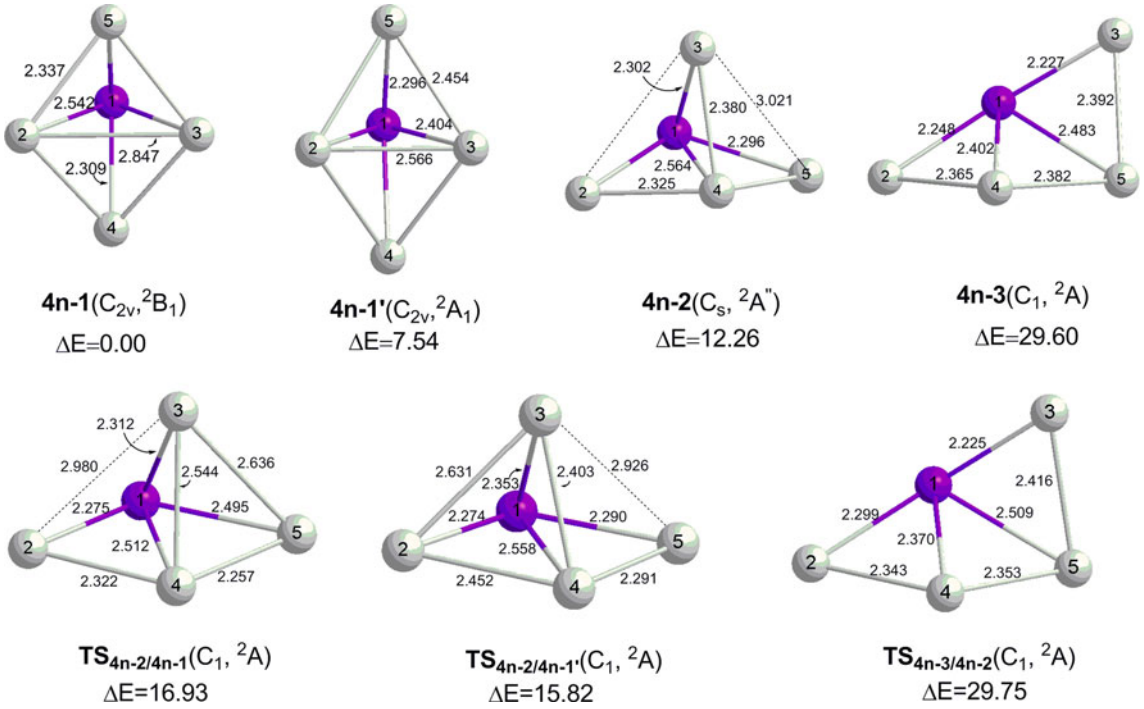

Fig. 3 Optimized geometries of the PSi_4 cluster and the corresponding transition state structures at the B3LYP/6-311+G* level

plus the additional one add up to 12, which accords with Wade's rules for $N = 5$, hence the trigonal bipyramid should be the most stable structure for PSi_4^-.

Figure 4 displays the lowest-unoccupied molecular orbital (LUMO) of PSi_4^+, and the highest-occupied molecular orbital (HOMO) of PSi_4 and PSi_4^-. All three orbitals are bonding ones and have similar orbital compositions, thus the greater the number of electrons in the orbitals, the more compact the base triangle, as predicted for the $PSi_4^+/PSi_4/PSi_4^-$ ground state structures.

As shown in Table 3, results given by B3PW91 for the $PSi_4/PSi_4^+/PSi_4^-$ isomers show some differences from those by B3LYP, especially for **4n-3**, **4c-2**, and **4c-3**. Isomer **4n-3** is not a stable minimum on the B3PW91 PES. An attempted geometry optimization of structure **4n-3** starting from the B3LYP optimized structure **4n-3** converges to structure **4n-2** with the B3PW91 method. Reducing the step size to 0.01 Bohr (the default is 0.30 Bohr) in the geometry optimizer or freezing the "reaction coordinate" between **4n-2** and **4n-3** (and then relaxing it) still resulted in structure **4n-2**. Single-point B3PW91 calculation at the B3LYP optimized structure **4n-3** gave a relative energy of 35.48 kcal/mol with respect to the ground state structure **4n-1**. The B3PW91 optimized structure **4n-2** with a relative energy 14.92 kcal/mol with respect to the ground state structure, **4n-1**, was used as a starting structure for a geometry optimization performed at the B3LYP level. The resulting structure **4n-2** is exactly same to the originally

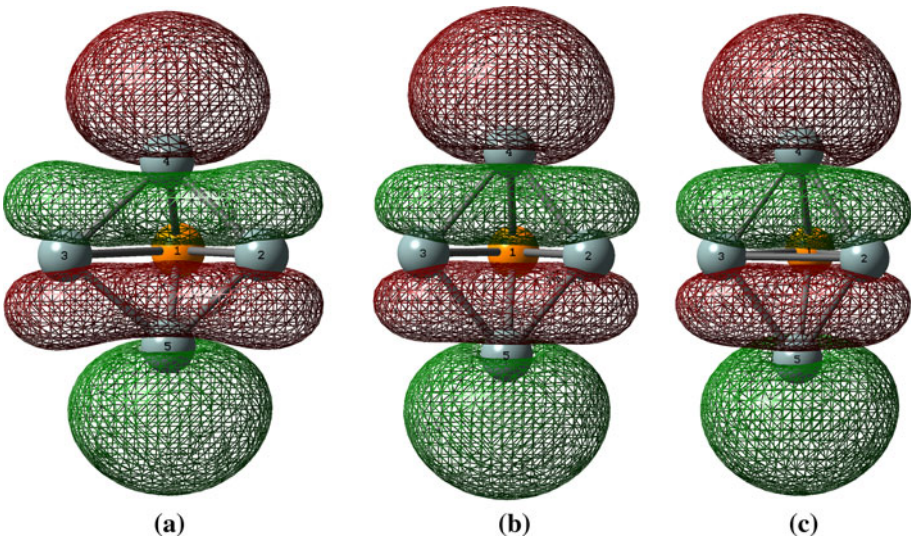

Fig. 4 Some frontier orbitals of PSi_4^+/PSi_4/PSi_4^-. **a** the LUMO of PSi_4^+, **b** the HOMO of PSi_4, and **c** the HOMO of PSi_4^-

B3LYP optimized structure **4n-2**. Note that the **4n-1** isomer is the lowest energy structure for both the B3PW91 and B3LYP functionals (on both the B3PW91 and B3LYP PESs).

It is known that DFT methods in general can underestimate barriers, and our work further documents that even similar XC functionals (i.e., B3LYP and B3PW91) can give very different results due to the barriers being different (and hence the topologies of their PESs). We determined the barrier between the **4n-3** and **4n-2** structures at the B3LYP level using the transition state search algorithms QST2 [73] (Electronic supplementary material) and QST3 [74]. Using the two methods, a transition state $\mathbf{TS_{4n\text{-}3/4n\text{-}2}}$ (Fig. 3) was found, which has one imaginary vibrational frequency at $80i$ cm^{-1}. Further intrinsic reaction coordinate analysis [75, 76] verifies that $\mathbf{TS_{4n\text{-}3/4n\text{-}2}}$ really connects **4n-3** and **4n-2**. Based on the energy of $\mathbf{TS_{4n\text{-}3/4n\text{-}2}}$, the barrier from **4n-3** to **4n-2** is only 0.13 kcal/mol, which may explain why structure **4n-3** cannot be obtained by the B3PW91 method. Using the same methods, the transition state structure $\mathbf{TS_{4n\text{-}2/4n\text{-}1}}$ (Fig. 3) (one imaginary frequency at $205i$ cm^{-1}) from **4n-2** to **4n-1** and the transition state structure $\mathbf{TS_{4n\text{-}2/4n\text{-}1'}}$ (Fig. 3) (one imaginary frequency at $223i$ cm^{-1}) from **4n-2** to **4n-1′** were also found, and the barriers are predicted to be 4.67 and 3.56 kcal/mol, respectively.

For Isomers **4c-2** and **4c-3,** B3PW91 predicts their relative energies are 11.49 and 12.38 kcal/mol with respect to the ground state **4c-1**, which are 3.24 and 2.70 kcal/mol energetically higher than the B3LYP results, respectively. The somewhat large energy differences may result from the different energy estimating ways of these two functionals. B3PW91 follows Eq. 1 to calculate the XC energy of one system [61–63]. With respect to correlation functional, PW91 takes Perdew and Wang's 1991 gradient-corrected correlation functional. The B3LYP XC energy [40] is defined by Eq. 2, where a, b, and c have the same values as in B3PW91, but the correlation functional, LYP, is designed to compute the full correlation energy, and not a correction to LSDA.

$$E_{XC}^{B3PW91} = (1-a)E_X^{LSDA} + aE_X^{HF} + b\Delta E_X^{B} + E_C^{LSDA} + c\Delta E_C^{PW91} \quad (1)$$

$$E_{XC}^{B3LYP} = (1-a)E_X^{LSDA} + aE_X^{HF} + b\Delta E_X^{B} + (1-c)E_C^{LSDA} + cE_C^{LYP}. \quad (2)$$

3.1.5 n = 5

The three minima for PSi_5, after geometric optimization, are presented according to their energies in Fig. 1. The two lower-energy structures, **5n-1** and **5n-2,** both favor the capped trigonal bipyramid (C_s), which differs from the crossed rhombus ground state predicted by Nigam et al. [33], but similar to that of Si_6 [34, 35]. It should be noted that Si_6 exhibited a fluxional behavior, fluctuating around a symmetric D_{4h} structure [36]. With different computational methods, three different structures (C_{2v} symmetry edge-capped trigonal bipyramid, C_s symmetry face-capped trigonal bipyramid, and D_{4h} symmetry distorted octahedron) are predicted for the ground state of Si_6 [34–36]. Structure **5n-2** is energetically less stable than **5n-1** by 1.35 kcal/mol; the P atom occupies one of the axial apexes of the trigonal bipyramid in **5n-1**, one of the vertices of the base triangle in **5n-2**. The P atom is, therefore, 3-coordinated in the former while 4-coordinated in the latter; the lower coordination position again seems favorable for the P atom. The structure with the P atom trapped in the same plane formed by all the Si atoms, **5n-3**, requires 17.65 kcal/mol more energy than the ground state **5n-1**.

Removal of an electron does not change the main configurations of the PSi_5 isomers but reverses their order of

stability, as illustrated in Fig. 1. Similar to the neutral **5n-2**, the lowest energy isomer, **5c-1,** of PSi_5^+ is a face-capped triangular bipyramid (C_s), with P at one of the vertices of the base triangle. The meta-stable isomer, **5c-2**, with 2.72 kcal/mol higher energy than **5c-1**, has a distorted C_s triangular bipyramid structure, similar to the neutral **5n-1**. The Si6-Si4-Si5-Si3 dihedral angle is enlarged from the 77.7° of **5n-1** to 123.6° of **5c-2**, which results in an increase of the Si3-Si6 distance from 2.616 Å (**5n-1**) to 3.513 Å (**5c-2**); the latter can be regarded as edge-capped, the former as a face-capped. The third isomer, **5c-3,** is a planar structure with energy 19.71 kcal/mol greater than **5c-1**.

Three lower-energy structures, **5a-1**, **5a-2,** and **5a-3** (Fig. 1), were found for the negatively charged PSi_5^- ion, differing in energy by less than 2.00 kcal/mol. Structure **5a-1** has the lowest energy and displays a C_{4v} tetragonal bipyramid structure, which is quite different from that of neutral PSi_5 and cationic PSi_5^+, but similar to that of Si_6^-. The framework of **5a-1** could also be explained by Wade's rules [71, 72]: for PSi_5^-, the total number of valence electrons, plus the additional one, adds up to 14, which accords with Wade's $2N+2$ rule for closed polyhedra for $N = 6$, hence the tetragonal bipyramid is preferred. Structure **5a-2**, a mere 0.82 kcal/mol energetically above **5a-1**, is a face-capped trigonal bipyramid, similar to the lowest-energy neutral structure, **5n-1**. The Si6-Si4-Si5-Si3 dihedral angle in **5a-2** is squeezed to 72.6°, compared with the 77.7° in **5n-1**. Structure **5a-3** results from capping the Si6 atom onto the P-Si4-Si5 surface instead of the Si3-Si4-Si5 surface used in **5a-2** and is 1.09 kcal/mol less stable than **5a-2**. The planar structure **5a-4**, similar to the planar structure **5n-3**, is 7.89 kcal/mol energetically above the global minimum, **5a-1**.

3.1.6 n = 6

The ground state structure of the PSi_6 cluster, **6n-1**, is a C_{2v} pentagonal bipyramid, similar to the Si_7^- cluster. The P atom prefers to replace one of the Si atoms in the base pentagon, as indicated in Fig. 2. For isomer **6n-2**, the P atom occupies the apex position, but this configuration requires 6.69 kcal/mol more energy than the **6n-1** form; thus, the P atom still prefers the lower coordination base atom over the higher coordination apex atom. Next in energy come three low-energy isomers, **6n-3**, **6n-4,** and **6n-5,** which all display di-face-capping trigonal bipyramid structures with the P atom in different positions. Again, the lower coordination position is favored for the P atom in these three similar isomers. Planar structures**,** with the P atom encapsulated by the Si atoms**,** were not found; all calculations converged to three-dimensional structures.

Similar to neutral PSi_6, cationic PSi_6^+ also adopts pentagonal bipyramid geometry as its ground state structure, **6c-1**, with the P atom occupying the same position as it does in **6n-1**. In contrast with **6n-1**, the base pentagon of **6c-1** becomes larger. Structure **6c-2**, 2.80 kcal/mol energetically less stable than **6c-1**, has a similar pentagonal bipyramid structure to **6c-1**, with the P atom occupying the apex position. Three other di-face-capping trigonal bipyramid structures, **6c-3**, **6c-4**, and **6c-5,** are 8.45, 10.70, and 13.48 kcal/mol, respectively, above the global minimum, **6c-1**.

The ground state of anionic PSi_6^-, **6a-1**, also retains the C_{2v} pentagonal bipyramid structure of the neutral and cationic clusters. However, from **6c-1** to **6n-1** to **6a-1**, the base pentagon becomes increasingly compressed due to their frontier orbitals; as illustrated in Fig. 5, the LUMO of PSi_6^+, the HOMO of PSi_6, and PSi_6^- have similar orbital compositions and, as all are bonding, additional electrons in the orbitals would compress the base pentagon. The PSi_6^- anion has 16 skeletal electrons; thus, Wade's $2N+2$ rule for closed polyhedra [71, 72] indicates a preferred pentagonal bipyramid structure ($N = 8$). The second stable structure, **6a-2,** a face-capped C_s tetragonal bipyramid structure is 4.81 kcal/mol higher in energy than **6a-1**. The C_{5v} pentagonal bipyramid, **6a-3**, with the P atom

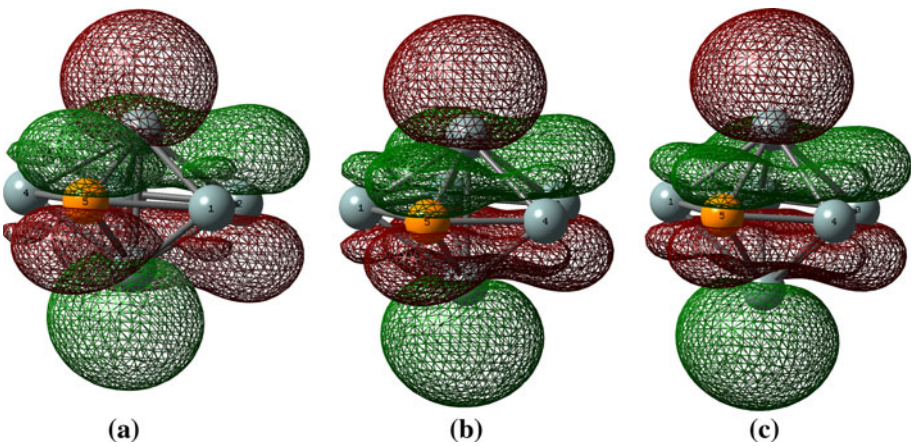

Fig. 5 Some frontier orbitals of $PSi_6^+/PSi_6/PSi_6^-$. **a** the LUMO of PSi_6^+, **b** the HOMO of PSi_6, and **c** the HOMO of PSi_6^-

occupying the apex position, is the third stable isomer, which lies 7.21 kcal/mol energetically above **6a-1**. Changing the position of the P atom in **6a-2** gives isomer **6a-4** with 8.45 kcal/mol higher energy than **6a-1**.

3.1.7 n = 7

Neutral PSi_7 favors the C_{3v} tri-capped trigonal bipyramid**, 7n-1,** as its ground state structure, which is obtained by capping the three adjacent faces of the bipyramid with three Si atoms (Fig. 2). The P atom in **7n-1** is at the 3-coordinated bipyramid axial vertex. When the P atom occupies the 6-coordinated vertex, as in **7n-2**, the structural stability decreases significantly; its energy is 10.93 kcal/mol higher than **7n-1**. Both **7n-1** and **7n-2** can also be viewed as possessing the same crossed bent rhombus structures as Si_8^- but with the P atom at a long diagonal vertex in **7n-1** and at a short diagonal vertex in **7n-2**. In such similar structures, the P atom seems to prefer the lower coordination (the long diagonal vertex) position. Another isomer, **7n-3**, which adopts a C_s bi-capped tetragonal bipyramid, exhibits 12.83 kcal/mol higher energy than that of the lowest energy isomer.

For PSi_7^+, four isomers are shown in Fig. 2; both **7c-1** and **7c-3** are bi-capped tetragonal bipyramid structures, which can be seen as "substitutional structures" of the Si_8 cluster [77]. The P atom is 3-coordinated in **7c-1,** while 5-coordinated in **7c-3**. Structure **7c-1** has the lowest energy; **7c-3** is 14.09 kcal/mol higher energetically. Both **7c-2** and **7c-4** exhibit tri-capped trigonal bipyramid structures, which can also be seen as crossed bent rhombi. The P atom locates at a long diagonal vertex in the former, a short diagonal vertex in the latter. Energetically, they are higher than the global minimum **7c-1**, by 6.31 and 14.13 kcal/mol, respectively. Isomer **7c-1** is structurally similar to **7n-3**, isomer **7c-2** to **7n-1**, indicating that removal of an electron from the neutral cluster changes the relative order of stability of the isomers.

For PSi_7^-, the ground state structure, **7a-1**, still favors the same C_{3v} tri-capped trigonal bipyramid as **7n-1**. When it is seen as the crossed rhombus, the P atom is found at a long diagonal vertex. If the P atom occupies a short diagonal vertex, the meta-stable configuration **7a-2** results with 14.57 kcal/mol more energy than **7a-1**. Isomer **7a-3** presents a bi-capped tetragonal bipyramid, 19.41 kcal/mol higher in energy than the ground state **7a-1**.

3.1.8 n = 8

Two low-energy structures, **8n-1** and **8n-2**, with very similar energies are found for the neutral PSi_8 cluster. Both of the configurations are distorted cubic structures with one Si atom capping the triangular face on the upper rhombus. The former is the ground state structure of PSi_8; the latter is higher in energy by only 1.33 kcal/mol. Structures **8n-1** and **8n-2** can also be regarded as the "substitutional structures" of the Si_9^- cluster [77], with the P atom replacing one Si atom at a long diagonal vertex of a rhombus. The main structural difference between **8n-1** and **8n-2** is that the P atom locates in the bottom bent rhombus of **8n-1,** in the upper of **8n-2**. The P atom connects with three Si atoms in **8n-1**, four in **8n-2**. Another isomer of PSi_8, **8n-3**, which is 4.64 kcal/mol higher in energy than **8n-1**, presents a significantly twisted cube, with the P atom capping the upper rhombus face. In this structure, the P atom is also 4-coordinated. Once more, for the PSi_8 cluster isomers, the P atom follows the same trend of occupying the lower coordination position (3-coordination over 4-coordination), as discussed above.

For PSi_8^+, four isomers are found, three of which exhibit a similar structural pattern to Si_9 [77], with the P atom occupying different positions. The ground state, **8c-1**, displays a distorted cubic (C_s) structure with one Si atom capping the upper rhombus face, which is somewhat different from **8n-1** as the capping Si atom is 4-coordinated in **8c-1,** while 3-coordinated in **8n-1**. The P atom occupies a long diagonal vertex of the bottom rhombus. Moving the P atom in **8c-1** to a short diagonal vertex of the bottom, or a long diagonal vertex of the upper rhombus, gives the isomers **8c-2** or **8c-3**, respectively. Structures **8c-2** and **8c-3** possess 6.82 and 9.93 kcal/mol higher energy, respectively, than the ground state, **8c-1**. The fourth isomer, **8c-4**, can also be regarded as a capped cube but having undergone significant distortion compared with the three former structures. The distances Si5–Si6, Si5–Si7 and P–Si4 in **8c-4** are largely elongated; the P atom caps a triangular face on the upper rhombus, and structure **8c-4** possesses 11.25 kcal/mol more energy than structure **8c−1**.

Two almost iso-energetic isomers, **8a-1** and **8a-2**, are predicted for the ground state of anionic PSi_8^-; both exhibit a tricapped trigonal prism (TTP) form: the P atom occupies a prism vertex in **8a-1,** but acts as a cap atom in **8a-2**, yielding a mere 0.29 kcal/mol energy difference. Having 20 skeletal electrons, structures **8a-1** and **8a-2** accord with Wade's rule [71, 72] for $2N+2$ electrons with $N = 9$; hence, the tricapped trigonal prism is favorable for PSi_8^-. The third stable structure, **8a-3**, corresponds to neutral **8n-1** and lies 3.01 kcal/mol higher in energy than the ground state, **8a-1**. Isomer **8a-4**, analogous with **8n-3**, but with large distortion, is 4.75 kcal/mol energetically less stable than **8a-1**.

3.2 Overall

Generally therefore, phophorus-doped silicon clusters, PSi_n, possess similar ground state structures to the Si_{n+1}^-

clusters, with the exception of $n = 5$, presumably as a result of having an equal number of electrons, plus the similar atomic radii of the P (1.1 Å) and Si (1.07 Å) atoms. The same holds for the cationic PSi_n^+ clusters, which correspond, electron-wise, to Si_{n+1}. For anionic PSi_n^- clusters, most of their lowest-energy structures conform to Wade's $2N+2$ rule for closed polyhedra [71, 72].

The low-energy isomers of ionic PSi_n^+ and PSi_n^- typically retain the structural motives of neutral PSi_n. However, the relative order of stability of the isomers is always changed, sometimes reversed mainly for the clusters with an odd number of Si atoms, when removing/adding an electron from/to neutral PSi_n. From cationic PSi_n^+ to neutral PSi_n to anionic PSi_n^-, the similar structures tend to be contracted along with reduction, indicating a strengthening of the interactions between atoms.

The results reveal that the P atom in neutral PSi_n prefers the lower coordination sites in analogous configurations. This may be related to the electronic configurations of the P and Si atoms. Silicon atom has two *3s* and two *3p* electrons. In general, it forms four covalent bonds with other atoms by adopting sp^3 hybrid orbitals. While the P atom has a $3s^2 3p^3$ electronic configuration and tends to form three bonds with other neighboring atoms after inequivalent sp^3 hybridization, just as it does in white phosphorus [78]. Repelled by the lone pair of electrons, the P atom always favors the lower coordination sites with smaller Si–P-Si angles. Nitrogen is in the same main group as P in the periodic table; thus, N and P atoms favor the same substitutional sites in doped Si_n clusters [31].

3.3 Electron affinities and ionization potentials

The ionization potential (IP) and the electron affinity (EA) values of the PSi_n clusters, as a function of the cluster size, are important quantities that reflect the stability of the clusters. EA is defined as the amount of energy released when an electron is added to a neutral molecule. A higher electron affinity means more energy is released when an electron is added to the neutral molecule; hence, the generation of the corresponding anion is more readily achieved. IP is defined as the amount of energy required to remove an electron from a molecule. A lower ionization potential means less energy is needed to remove an electron from the neutral molecule; thus, the generation of the corresponding cationic isomer is more feasible.

Fig. 6 depicts the variations of the adiabatic EA (AEA) and the adiabatic IP (AIP) of the PSi_n (n = 1–8) clusters with the number of silicon atoms, n. The AEA and AIP herein are calculated as:

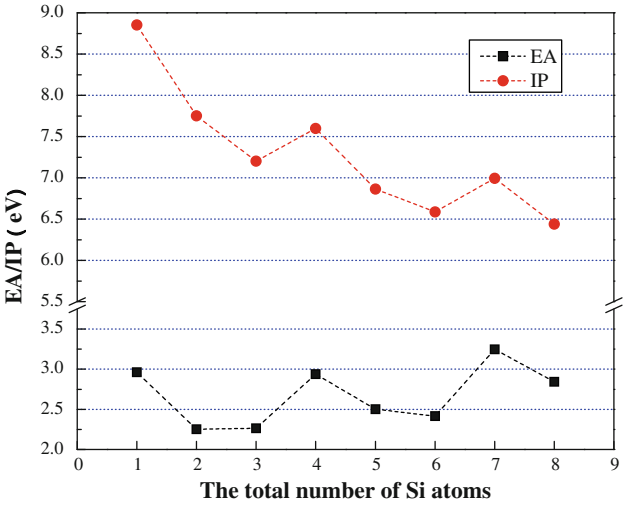

Fig. 6 The dependence of adiabatic electron affinity and adiabatic ionization potential for the lowest energy structures on the total number of Si atoms n

$$\mathrm{AEA} = E(\text{optimized neutral}) - E(\text{optimized anion}) \quad (3)$$

$$\mathrm{AIP} = E(\text{optimized cation}) - E(\text{optimized neutral}) \quad (4)$$

When $n = 4$ and 7, the AEA and AIP values are higher than those of adjacent clusters, reflecting the higher stability of the PSi_4^- and PSi_7^- anions, and the difficulty in forming PSi_4^+ and PSi_7^+ cations. The AIP values tend to decrease as n increases. For PSi_3 and PSi_6, the AIPs are lower than those of adjacent clusters, implying that the PSi_3 and PSi_6 clusters easily lose an electron to form the PSi_3^+ and PSi_6^+ cations.

3.4 Binding energy

In order to understand the relative stability of the PSi_n, PSi_n^-, and PSi_n^+ clusters, the binding energy (BE) per atom has been plotted in Fig. 7 as a function of the total number of Si atoms, n. These binding energies are determined as follows:

$$\mathrm{BE}(PSi_n) = [n \times E(\mathrm{Si}) + E(\mathrm{P}) - E(PSi_n)]/(n+1) \quad (5)$$

$$\mathrm{BE}(PSi_n^-) = [n \times E(\mathrm{Si}) + E(\mathrm{P}-) - E(PSi_n^-)]/(n+1) \quad (6)$$

$$\mathrm{BE}(PSi_n^+) = [(n-1) \times E(\mathrm{Si}) + E(Si^+) + E(\mathrm{P}) - E(PSi_n^+)]/(n+1) \quad (7)$$

Binding energy increases sharply for very small clusters before plateauing for larger clusters, with small humps or dips for specific cluster sizes indicating their relative

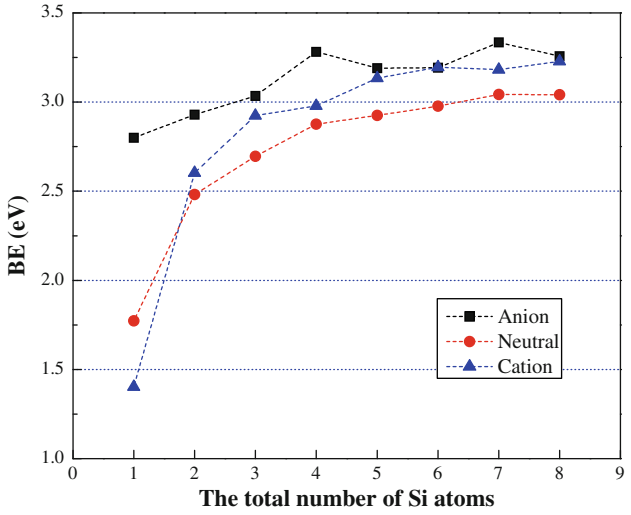

Fig. 7 The size dependence of binding energy for the lowest energy structures

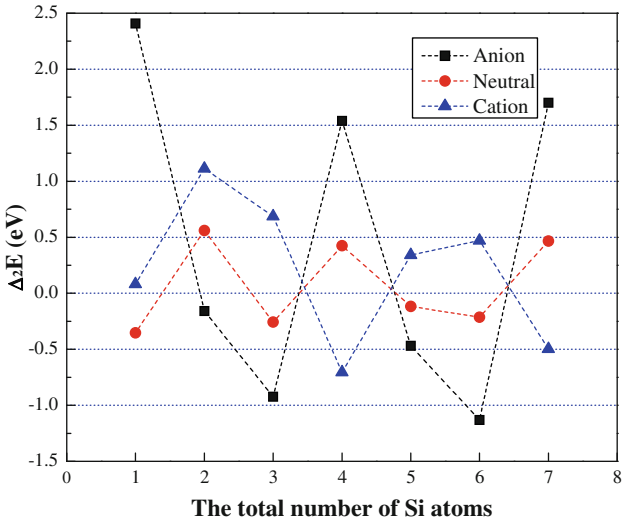

Fig. 8 The size dependence of second-order difference energy for the lowest energy structures

stabilities. There are local peaks at $n = 4$, and 7 for the anions, implying that these clusters are more stable than their neighbors. While for the neutral and the cationic clusters, the fluctuation is less pronounced.

3.5 The second-order energy difference

The second-order energy difference of a cluster, Δ_2E, is a sensitive quantity reflecting the stability of clusters, which is defined as:

$$\Delta_2 E(\mathrm{PSi}_n) = E(\mathrm{PSi}_{n+1}) + E(\mathrm{PSi}_{n-1}) - 2E(\mathrm{PSi}_n) \quad (8)$$

$$\Delta_2 E(\mathrm{PSi}_n^-) = E(\mathrm{PSi}_{n+1}^-) + E(\mathrm{PSi}_{n-1}^-) - 2E(\mathrm{PSi}_n^-) \quad (9)$$

$$\Delta_2 E(\mathrm{PSi}_n^+) = E(\mathrm{PSi}_{n+1}^+) + E(\mathrm{PSi}_{n-1}^+) - 2E(\mathrm{PSi}_n^+). \quad (10)$$

From the expressions above, it is clear that the clusters with positive values of $\Delta_2 E$ are more stable than their nearest neighbors. $\Delta_2 E$ for PSi_n, PSi_n^- and PSi_n^+ clusters as a function of cluster size is plotted in Fig. 8.

Maxima are found at $n = 2$, 4, and 7 for the neutrals and at $n = 4$, and 7 for the anions, respectively, indicating higher stabilities, consistent with the binding energies presented in Fig. 7. For the cations, small humps occur for $n = 2$, and 6, revealing their relatively higher stabilities in comparison to their neighbors, while the $\Delta_2 E$ values are minima and negative when $n = 4$, and 7, implying that these two clusters are unstable.

3.6 *HOMO-LUMO gaps*

The HOMO-LUMO gap, the energy difference between the highest-occupied and the lowest-unoccupied molecular orbitals, is a characteristic quantity of electron structures. We should note that KS orbitals were originally introduced only as a practical tool and have no physical meaning initially [79]. Many researchers have discussed on whether or not we could relate the orbital energies emerged from a KS calculation with the IP and the EA [80–85]. It has been found that there is a reasonable approximation between the KS HOMO-LUMO difference and the lowest excitation energy [86–89]. Molecules with large HOMO-LUMO gaps are generally stable and unreactive; while those with small gaps are generally reactive.

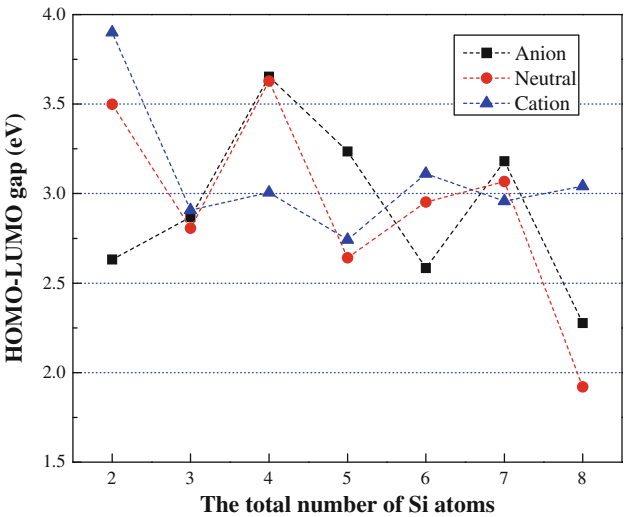

Fig. 9 The size dependence of the HOMO-LUMO gap for the lowest energy structures

As presented in Fig. 9, anionic PSi_4^- and PSi_7^- have larger HOMO-LUMO gaps, indicating their relatively higher stabilities, in agreement with the binding energy

results of Fig. 7. This is also the case for neutral PSi_4 and PSi_7, while for the cations, the humps occur at $n = 4$, and 6, but are less pronounced.

4 Conclusions

The structures and stabilities of charged phosphorus-doped small silicon clusters PSi_n^+/PSi_n^- ($n = 1$–8) have been investigated by the density functional theory (DFT-B3LYP) method in conjunction with the 6-311+G* basis sets. The PSi_n^+ cations generally follow structural patterns similar to those of pure Si_{n+1} clusters, except $n = 5$. The structures are planar for n $\leq$3, tridimensional when $n > 3$. Cationic PSi_2^+ and PSi_3 favor open isosceles triangle and planar rhombus structures, respectively. For PSi_4^+, PSi_5^+, PSi_6^+, PSi_7^+ and PSi_8^+, the ground state structures possess trigonal bipyramidal, face-capped trigonal bipyramidal, pentagonal bipyramidal, bi-faced-capped tetragonal bipyramidal, and capped distorted cubic structures, respectively. For anionic PSi_n^-, most of the lowest-energy structures accord with Wade's $2N+2$ rule for closed polyhedra: trigonal bipyramid, tetragonal bipyramid, pentagonal bipyramid, and tricapped trigonal prism (TTP) structures are favored for PSi_4^-, PSi_5^-, PSi_6^-, and PSi_8^-, respectively, corresponding to Wade's rule of $2N+2$ with $N = 5$, 6, 7, and 9. Adding an electron compacts structures from cationic PSi_n^+ to neutral PSi_n to anionic PSi_n^-, implying a strengthening of the interactions between atoms with an increasing number of electrons in the clusters. Furthermore, the relative stability order of the PSi_n^+/PSi_n^- isomers is always changed, sometimes reversed mainly for the clusters with an odd number of Si atoms, compared with the PSi_n isomers.

The stabilities of the clusters were also analyzed by their AIP, AEA, BE, Δ_2E, and HOMO-LUMO gap values, which indicated that the PSi_4^- and PSi_7^- clusters have higher stability than their neighboring clusters for anionic PSi_n^-. For the cations, the stability differences are not clearly predicted by their binding energies. However, based on their Δ_2E and HOMO-LUMO gap values, the PSi_6^+ cluster is more stable than the neighbors.

Acknowledgments This research was supported by the 973 program (2009CB226109) in China and Guangdong provincial natural science foundation (10151063101000041) of China. Dr. David E. Finlow provided a critical reading of the manuscript, plus assistance with the English. Specially thank the last reviewer for his/her series of worthwhile suggestions that make our work have an improvement.

References

1. Bloomfield LA, Freeman RR, Brown WL (1985) Phys Rev Lett 54:2246–2249
2. Jarrold MF (1991) Science **252**: 1085–1092. http://www.jstor.org/stable/2876284
3. Pouchan C, Begue D, Zhang DY (2004) J Chem Phys 121:4628–4634
4. Ho KM, Shvartsburg AA, Pan B, Lu ZY, Wang CZ, Wacker JG, Fye J, Jarrold MF (1998) Nature 392:582–584
5. Hagelberg F, Leszczynski J, Murashov V (1998) J Mol Struct Theochem 454:209–216
6. Rata I, Shvartsburg AA, Horoi M, Frauenheim T, Siu KWM, Jackson KA (2000) Phys Rev Lett 85:546–549
7. Kanayama T (1994) Jpn J Appl Phys 33:1792–1795
8. Kanayama T, Murakami H (1997) J Vac Sci Technol B 15:2882–2886
9. Guo P, Zhao YR, Wang F, Jiang B, Han JG, Wang GH (2004) J Chem Phys 121:12265–12275
10. Beck SM (1989) J Chem Phys 90:6306–6312
11. Hiura H, Miyazaki T, Kanayama T (2001) Phys Rev Lett 86:1733–1736
12. Kumar V, Kawazoe Y (2001) Phys Rev Lett 87:045503. doi:10.1103/PhysRevLett.87.045503
13. Kumar V, Kawazoe Y (2002) Phys Rev B 65:073404. doi:10.1103/PhysRevB.65.073404
14. Xiao CY, Hagelberg F Jr (2002) Phys Rev B 66:075425. doi:10.1103/PhysRevB.66.075425
15. Li M, Zhao JJ, Wang JG, Wang BL, Lu QL, Wang GH (2006) Phys Rev B 73:125439. doi:10.1103/PhysRevB.73.125439
16. Li JR, Wang GH, Yao CH, Mu YW, Wan JG, Han M (2009) J Chem Phys 130:164514. doi:10.1063/1.3123805
17. Sen P, Mitas L (2003) Phys Rev B 68:155404. doi:10.1103/PhysRevB.68.155404
18. Koyasu K, Atobe J, Mitsui M, Nakajima A (2007) J Phys Chem A 111:42–49
19. Kishi R, Iwata S, Nakajima A, Kaya K (1997) J Chem Phys 107:3056–3070
20. Wei S, Barnett RN, Landman U (1997) Phys Rev. B 55:7935–7944
21. Sporea C, Rabilloud F, Allouche AR, Frecon M (2006) J Phys Chem A 110:1046–1051
22. Sporea C, Rabilloud F, Cosson X, Allouche AR, Frecon M (2006) J Phys Chem A 110:6032–6038
23. Lin LH, Yang JC, Ning HM, Hao DS, Fan HW (2008) J Mol Struct Theochem 851:197–206
24. Hao DS, Liu JR, Wu WG, Yang JC (2009) Theor Chem Acc 124:431–437
25. Majumder C, Kulshreshtha SK (2004) Phys Rev B 69:115432. doi:10.1103/PhysRevB.69.115432
26. Nigam S, Majumder C, Kulshreshtha SK (2004) J Chem Phys 121:7756–7763
27. Li BX, Wang GY, Ye MY, Yang GC, Yao CH (2007) J Mol Struct Theochem 820:128–140
28. Fang HW, Yang JC, Lu W, Ning HM, Zhang QC (2010) J Phys Chem A 114:1218–1223
29. Chu QY, Li BX, Yu J (2007) J Mol Struct Theochem 806:67–76
30. Jackson K, Jungnickel G, Frauenheim T (1998) Chem Phys Lett 292:235–242
31. Li BX, Wang GY, Ding WF, Ren XJ, Ye JZ (2009) Phys B 404:1679–1685
32. Jungnickel G, Frauenheim T, Jackson KA (2000) J Chem Phys 112:1295–1305
33. Nigam S, Majumder C, Kulshreshtha SK (2006) J Chem Phys 125:074303
34. Zdetsis AD (2001) Phys Rev A 64:023202
35. Zhao CY, Balasubramanian K (2002) J Chem Phys 116:3690–3799
36. Zdetsis AD (2007) J Chem Phys 127:014314. doi:10.1063/1.2746030

37. Frisch MJ, Trucks GW, Schlegel HB, Scuseria GE, Robb MA, Cheeseman JR, Montgomery Jr. JA, Vreven T, Kudin KN, Burant JC, Millam JM, Iyengar SS, Tomasi J, Barone V, Mennucci B, Cossi M, Scalmani G, Rega N, Petersson GA, Nakatsuji H, Hada M, Ehara M, Toyota K, Fukuda R, Hasegawa J, Ishida M, Nakajima T, Honda Y, Kitao O, Nakai H, Klene M, Li X, Knox JE, Hratchian HP, Cross JB, Bakken V, Adamo C, Jaramillo J, Gomperts R, Stratmann RE, Yazyev O, Austin AJ, Cammi R; Pomelli C, Ochterski JW, Ayala PY, Morokuma K, Voth GA, Salvador P, Dannenberg JJ, Zakrzewski VG, Dapprich S, Daniels AD, Strain MC, Farkas O, Malick DK, Rabuck AD, Raghavachari K, Foresman JB, Ortiz JV, Cui Q, Baboul AG, Clifford S, Cioslowski J, Stefanov BB, Liu G, Liashenko A, Piskorz P, Komaromi I, Martin RL, Fox DJ, Keith T, Al-Laham MA, Peng CY, Nanayakkara A, Challacombe M, Gill PMW, Johnson B, Chen W, Wong MW, Gonzalez C, Pople JA *Gaussian 03*, Revision D.01, Gaussian, Inc., Wallingford, CT, 2003
38. Stephens PJ, Devlin FJ, Chabalowski CF, Frisch MJ (1994) J Phys Chem 98:11623–11627
39. Becke D (1993) J Chem Phys 98:5648–5652
40. Lee C, Yang W, Parr RG (1988) Phys Rev B 37:785–789
41. Guo LJ, Liu X, Zhao GF, Luo YH (2007) J Chem Phys 126:234704. doi:10.1063/1.2743412
42. Han JG, Zhao RN, Duan YH (2007) J Phys Chem A 111:2148–2155
43. Lan YZ, Feng YL (2009) Phys Rev A 79:033201. doi:10.1103/PhysRevA.79.033201
44. Ngan VT, Gruene P, Claes P, Janssens E, Fielicke A, Nguyen MT, Lievens P (2010) J Am Chem Soc 132:15589–15602
45. McLean AD, Chandler GS (1980) J Chem Phys 72:5639–5648
46. Frisch MJ, Pople JA J, Binkley S (1984) J Chem Phys 80:3265–3269
47. Johnson BG, Frisch MJ (1993) Chem Phys Lett 216:133–140. doi:10.1016/0009-2614(93)E1238-C
48. Stratmann RE, Burant JC, Scuseria GE, Frisch MJ (1997) J Chem Phys 106:10175–10183. doi:10.1063/1.474047
49. Kasdan A, Herbst E, Lineberger WC (1975) J Chem Phys 62:541–548
50. Moore CE (1970) Natl Stand Ref Data Ser (U.S. Natl. Bur. Stand.) 34:1–44
51. Bennett SL, Margrave JL, Franklin JL (1974) J Chem Phys 61:1647–1651
52. Scheer M, Bilodeau RC, Brodie CA, Haugen HK (1998) Phys Rev A 58:2844–2856
53. Arnold CC, Kitsopoulos TN, Neumark DM (1993) J Chem Phys 99:766–768
54. Liu Z, Davies PB (1996) J Chem Phys 105:3443–3449
55. Guillaume M, Champagne B, Bégué D, Pouchan C (2009) J Chem Phys 130:134715-1-7
56. Truhlar DG (1993) J Chem Phys 98:2491
57. Zhao Y, Truhlar DG (2006) J Chem Theory Comput 2:1009–1018
58. Zhao Y, Truhlar DG (2006) J Phys Chem A 110:5121–5129
59. Zhao Y, Truhlar DG (2008) Acc Chem Res 41:157–167
60. Zhao Y, Truhlar DG (2007) J Am Chem Soc 129:8440–8442
61. Perdew JP, Chevary JA, Vosko SH, Jackson KA, Pederson MR, Singh DJ, Fiolhasis C (1992) Phys Rev B 46:6671–6687
62. Becke AD (1993) J Chem Phys 98:5648–5652
63. Perdew JP, Burke K, Wang Y (1996) Phys Rev B 54:533–539
64. Filatov M, Cremer D (2005) J Chem Phys 123:124101-1-7
65. Bartlett RJ, Lotrich VF, Schweigert IV (2005) J Chem Phys 123:062205-1-21
66. Bartlett RJ, Schweigert IV, Lotrich VF (2006) J Mol Struct Theochem 771:1–8
67. Yanai T, Tew DP, Handy NC (2004) Chem Phys Lett 393:51–57
68. Peach MJG, Helgaker T, Sałek P, Keal TW, Lutnæs OB, Tozer DJ, Handy NC (2006) Phys Chem Chem Phys 8:558–562. doi:10.1039/b511865d
69. Peach MJG, Cohen AJ, Tozer DJ (2006) Phys Chem Chem Phys 8:4543–4549
70. Jakubek ZJ, Nakhate SG, Simard B (2002) J Chem Phys 116:6513–6520
71. Wade K (1971) J Chem Soc D 792–793. doi:10.1039/C29710000792
72. Wade K (1976) Adv Inorg Chem 18:1–66. doi:10.1016/S0065-2792(08)60027-8
73. Peng C, Schlegel HB (1993) Isr J Chem 33:449–454
74. Peng C, Ayala PY, Schlegel HB, Frisch MJ (1996) J Comp Chem 17:49–56
75. Gonzalez C, Schlegel HB (1989) J Chem Phys 90:2154–2161
76. Gonzalez C, Schlegel HB (1990) J Phys Chem 94:5523–5527
77. Yang JC, Xu WG, Xiao WS (2005) J Mol Struct Theochem 719:89–102
78. Huang RB, Li HD, Lin ZY, Yang SH (1995) J Phys Chem 99:1418–1423
79. Parr RG, Yang W (1989) Density Functional Theory of Atoms and Molecules. New York, Oxford University Press
80. Baerends EJ, Gritsenko OV (1997) J Phys Chem A 101:5383–5403
81. Stowasser R, Hoffman R (1999) J Am Chem Soc 121:3414–3420
82. Tozer DJ, Proft FD (2005) J Phys Chem A 109:8923–8929
83. Zhang G, Musgrave CB (2007) J Phys Chem A 111:1554–1561
84. Kleinman L (1997) Phys Rev B 56:12042–12049
85. Kleinman L (1997) Phys Rev B 56:16029–16030
86. Wang Z, Day PN, Pachter R (1998) J Chem Phys 108:2504–2510
87. Mitsui M, Ohshima Y (2000) J Phys Chem A 104:8638–8648
88. Hutchison GR, Ratner MA, Marks TJ (2002) J Phys Chem A 106:10596–10605
89. Vargas R, Garza J, Cedillo A (2005) J Phys Chem A 109:8880–8892